



J. Ljungvall,<sup>1,2,3</sup> A. Görgen,<sup>1</sup> A. Obertelli,<sup>1</sup> W. Korten,<sup>1</sup> E. Clément,<sup>2</sup> G. de France,<sup>2</sup> A. Bürger,<sup>4</sup>  
 J.-P. Delaroche,<sup>5</sup> A. Dewald,<sup>6</sup> A. Gadea,<sup>7</sup> L. Gaudefroy,<sup>5</sup> M. Girod,<sup>5</sup> M. Hackstein,<sup>6</sup> J. Libert,<sup>8</sup>  
 D. Mengoni,<sup>9</sup> F. Nowacki,<sup>10</sup> T. Pissulla,<sup>6</sup> A. Poves,<sup>11</sup> F. Recchia,<sup>12</sup> M. Rejmund,<sup>2</sup> W. Rother,<sup>6</sup> E. Sahin,<sup>12</sup>  
 C. Schmitt,<sup>2</sup> A. Shrivastava,<sup>2</sup> K. Sieja,<sup>10</sup> J.J. Valiente-Dobón,<sup>12</sup> K.O. Zell,<sup>6</sup> and M. Zielińska<sup>13</sup>

<sup>1</sup>CEA Saclay, IRFU, Service de Physique Nucléaire, F-91191 Gif-sur-Yvette, France

<sup>2</sup>GANIL, CEA/DSM-CNRS/IN2P3, Bd Henri Becquerel, BP 55027, F-14076 Caen, France

<sup>3</sup>CSNSM, CNRS/IN2P3, F-91405 Orsay, France

<sup>4</sup>Department of Physics, University of Oslo, PO Box 1048 Blindern, N-0316 Oslo, Norway

<sup>5</sup>CEA, DAM, DIF, F-91297 Arpajon, France

<sup>6</sup>Institut für Kernphysik, Universität zu Köln, D-50937 Köln, Germany

<sup>7</sup>Instituto de Física Corpuscular, CSIC-Universidad de Valencia, E-46071 Valencia, Spain

<sup>8</sup>Institut de Physique Nucléaire, CNRS/IN2P3-Université Paris-Sud, F-91406 Orsay, France

<sup>9</sup>Dipartimento di Fisica dell'Università and INFN Sezione di Padova, I-35131 Padova, Italy

<sup>10</sup>IPHC, CNRS/IN2P3 and Université Louis Pasteur, F-67037 Strasbourg, France

<sup>11</sup>Departamento de Física Teórica, IFT-AM/CSIC, Universidad Autónoma, E-28049 Madrid, Spain

<sup>12</sup>INFN, Laboratori Nazionali di Legnaro, I-35020 Legnaro, Italy

<sup>13</sup>Heavy Ion Laboratory, Warsaw University, Warsaw, PL-02097, Poland

(Dated: May 11, 2010)

The lifetimes of the first excited  $2^+$  states in  $^{62}\text{Fe}$  and  $^{64}\text{Fe}$  have been measured for the first time using the recoil-distance Doppler shift method after multi-nucleon transfer reactions in inverse kinematics. A sudden increase of collectivity from  $^{62}\text{Fe}$  to  $^{64}\text{Fe}$  is observed. The experimental results are compared with new large-scale shell model calculations and Hartree-Fock-Bogolyubov-based configuration-mixing calculations using the Gogny D1S interaction. The results give a deeper understanding of the mechanism leading to an onset of collectivity near  $^{68}\text{Ni}$ , which is compared with the situation in the so-called *island of inversion* around  $^{32}\text{Mg}$ .

PACS numbers: 21.10.Re Collective levels 21.10.Tg Lifetimes 27.50.+e  $59 \leq A \leq 89$

It is a common feature of systems of interacting fermions to form a shell structure. In atomic nuclei the spin-orbit interaction lowers the energy of the orbitals with highest angular momentum into the next lower oscillator shell with opposite parity, leading to the well-known sequence of magic numbers. While the shell structure and the resulting energy gaps between the orbitals explain many general properties of nuclei across the nuclear chart, it has become evident that the shell structure and magic numbers change for nuclei with large neutron excess. As protons and neutrons in such exotic nuclei occupy different orbitals compared to their stable counterparts, the effective single-particle energies are shifted, so that some shell gaps vanish and new ones emerge [1]. It is important to find experimental signatures for the changing shell structure in order to advance the theoretical description of exotic nuclei, *e.g.* by finding better shell model interactions or better energy functionals for mean-field based models.

The region of neutron-rich nuclei between  $Z = 20$  (Ca) and  $Z = 28$  (Ni) is of particular interest for understanding the evolution of the shell structure for nuclei with large neutron excess. Adding protons to the  $1f_{7/2}$  orbital changes the relative energies of the neutron  $2p_{3/2}$ ,  $2p_{1/2}$ , and  $1f_{5/2}$  orbitals due to the strongly attractive proton-neutron spin-flip interaction [2]. With the gradual filling of the neutron  $fp$  harmonic oscillator shell, excitations into the  $1g_{9/2}$  intruder orbital become increasingly

important. Subtle effects related to the energy gap between the  $fp$  shell and the  $1g_{9/2}$  orbital lead to a strong variation of collectivity for nuclei with  $N \approx 40$ . The nucleus  $^{68}\text{Ni}_{40}$  has many features of a doubly-magic nucleus with high excitation energy of the  $2_1^+$  state [3] and a small  $B(E2; 0_1^+ \rightarrow 2_1^+)$  value [4]. Mass measurements, on the other hand, show that the  $N = 40$  gap is weak for  $^{68}\text{Ni}$  [5, 6], and it has been argued that the small  $B(E2)$  value does not necessarily indicate a shell gap at  $N = 40$ , but that it reflects the character of the  $2_1^+$  state as a predominant neutron excitation [7]. The fragility of the  $N = 40$  sub-shell gap is further evidenced by the developing collectivity in the neutron-rich Zn and Ge isotopes, for which the energy of the  $2_1^+$  state drops sharply from  $N = 38$  to  $N = 42$  while the  $B(E2)$  values increase [8, 9]. The removal of protons from the  $f_{7/2}$  orbital has a similar effect. The  $2_1^+$  energies in the Fe isotopes drop sharply above  $N = 36$ . The removal of only two protons changes the energy of the  $2_1^+$  state from 2033 keV in  $^{68}\text{Ni}$  to 573 keV in  $^{66}\text{Fe}$  [10]. The  $2_1^+$  energy drops even further to 517 keV in  $^{68}\text{Fe}$  [11]. A similar behavior is observed in the Cr isotopes, where the  $2_1^+$  energies decrease gradually beyond the  $N = 32$  sub-shell closure [12]. Inelastic proton scattering experiments [13] and shell model studies [14] corroborate the development of substantial collectivity and deformation in the neutron-rich Cr isotopes.

The role of the  $\nu g_{9/2}$  orbital for the onset of collectivity in the region below  $^{68}\text{Ni}$  has been discussed contro-

versially in the past. The excitation spectrum of  $^{64}\text{Fe}$  was established by Hoteling *et al.* and compared to shell model calculations restricted to the *fp* model space [15]. Since the calculations reproduced the energy of the  $2^+$  state reasonably well, it was concluded that the  $\nu g_{9/2}$  orbital is not responsible for the low  $2_1^+$  energy and that it becomes important only at higher energies, where the calculations could not reproduce the observed states. Lunardi *et al.* have studied neutron-rich Fe isotopes of both even and odd mass [16]. Comparing the results to shell model calculations in the *fpq* model space it was concluded that the occupation of the  $g_{9/2}$  orbital influences the structure of the neutron-rich Fe isotopes considerably. The increasing role of the  $g_{9/2}$  orbital is also consistent with the decreasing excitation energy of  $9/2^+$  isomers in odd-mass Fe nuclei [17]. In studies of the odd-mass Mn isotopes, Valiente-Dobón *et al.* have argued that including the effects of the  $g_{9/2}$  orbital improves the shell model description of  $^{61}\text{Mn}_{36}$  and  $^{63}\text{Mn}_{38}$  [18], while Crawford *et al.* have interpreted the level structure in  $^{61}\text{Mn}$  with a low level density below 1 MeV without the need to invoke neutron excitations into the  $g_{9/2}$  orbital [19]. In the Cr isotopes there is clear evidence for the influence of the  $g_{9/2}$  orbital already for  $^{59}\text{Cr}_{35}$  [20].

A deeper understanding of how collectivity develops in this region of the nuclear chart can come from experimental  $B(E2)$  values. For the even-even nuclei  $B(E2)$  values have been measured up to  $^{58}\text{Cr}_{34}$  [21],  $^{60}\text{Fe}_{34}$  [22], and  $^{70}\text{Ni}_{40}$  [23]. Here we report on a lifetime measurement for the  $2_1^+$  states in  $^{62}\text{Fe}$  and  $^{64}\text{Fe}$  performed at the *Grand Accelérateur National d'Ions Lourds* using the recoil-distance Doppler shift (RDDS) method [24] in combination with multi-nucleon transfer reactions in inverse kinematics. The technique is similar to the one used in a recent lifetime measurement in  $^{50}\text{Ca}$  and  $^{51}\text{Sc}$  in direct kinematics at Legnaro [25]. Excited states in a wide range of neutron-rich nuclei were populated in multi-nucleon transfer reactions between a  $^{238}\text{U}$  beam at 6.5A MeV and a  $^{64}\text{Ni}$  target of 1.5 mg/cm<sup>2</sup> thickness. The target-like reaction products were detected and identified event by event in the large-acceptance spectrometer VAMOS [26]. The optical axis of the spectrometer was positioned at 45° with respect to the beam axis, close to the grazing angle of the reaction. The focal plane detection system of the spectrometer allows the full reconstruction of the trajectories through the spectrometer and an unambiguous identification of the reaction products in mass, charge, and atomic number (see Fig. 1). The magnetic rigidity of the spectrometer was optimized for the transmission of  $^{64}\text{Fe}$ .

The target was surrounded by nine large, segmented germanium clover detectors of the Exogam array [27], one at 180°, three at 135°, and five at 90° relative to the spectrometer axis. The typical average recoil velocity of the target-like reaction products exiting the target foil was 37  $\mu\text{m}/\text{ps}$ . In order to apply the RDDS technique the velocity of the recoils was slowed to approximately 32  $\mu\text{m}/\text{ps}$  in a 4.7 mg/cm<sup>2</sup> thick magnesium foil

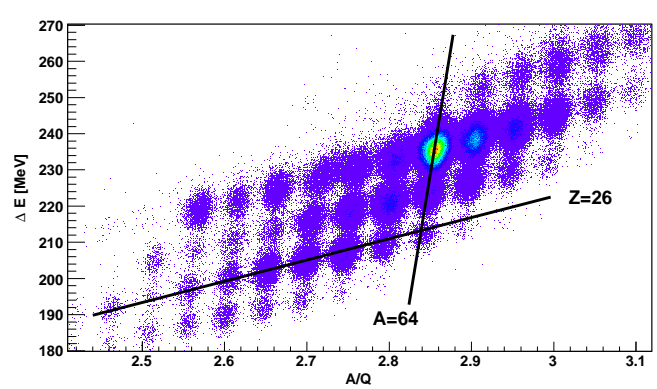


FIG. 1: Typical identification plot showing the energy loss of the ions in the ionization chamber of VAMOS as a function of the mass-over-charge ratio, which is determined from the time of flight through the spectrometer and the magnetic rigidity. The loci of ions with  $A = 64$  and  $Z = 26$ , respectively. The most intense peak corresponds to elastically scattered  $^{64}\text{Ni}$  target nuclei. The data is shown for only one of 21 silicon detectors mounted in VAMOS and for one single charge state ( $Q=23$ ). The identification of the ions was performed in the same way for all detectors and all charge states reaching the focal plane.

placed at micrometer distances behind the target. The different Doppler shifts of  $\gamma$  rays emitted before and after the degrader foil were measured in the germanium detectors under backward angles. The distance between target and degrader was adjusted and controlled by a compact *plunger* device [28]. Data was collected for six distances between 40 and 750  $\mu\text{m}$ . An additional measurement was performed without degrader to determine the exact recoil velocities after the target.

The spectra of Fig. 2 show  $\gamma$  rays recorded in coincidence with ions identified as  $^{62}\text{Fe}$  and  $^{64}\text{Fe}$  for selected target-degrader distances. A Doppler correction was performed using the recoil velocity measured in VAMOS after the degrader foil and the relative angle between the  $\gamma$  ray and the recoil vector. Two peaks are observed for the  $2_1^+ \rightarrow 0_1^+$  transitions in both  $^{62}\text{Fe}$  and  $^{64}\text{Fe}$ , corresponding to the different recoil velocities before and after the degrader foil, respectively. The peaks are well separated for relative angles greater than 135°. Spectra were produced and analyzed separately for two angular ranges between 135° and 150° and between 160° and 180°, respectively. Decay curves  $I_d/(I_d + I_f)$  were constructed from the intensities of the degraded ( $I_d$ ) and fully Doppler shifted ( $I_f$ ) components of the transitions as a function of target-degrader distance. The normalization factors ( $I_d + I_f$ ) were found to be consistent with the number of ions identified in VAMOS for each distance. Lifetimes of the  $2_1^+$  states in  $^{60}\text{Fe}$ ,  $^{62}\text{Fe}$ , and  $^{64}\text{Fe}$  were extracted separately for the two angular ranges from the decay curves of the  $2_1^+$  and  $4_1^+$  states using the differential decay curve (DDC) method [24] and then combined into a weighted average. In the DDC method the lifetime of a state is determined for each target-degrader distance from the

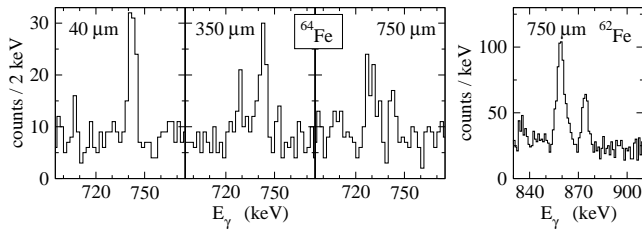


FIG. 2: Spectra showing the fully Doppler shifted and de-graded components of the  $2_1^+ \rightarrow 0_1^+$  transitions for three target-degrader distances in  $^{64}\text{Fe}$  and for one distance in  $^{62}\text{Fe}$ . The  $\gamma$  rays were observed at angles ranging from  $160^\circ$  to  $180^\circ$  with respect to the recoil direction.

slope of the decay curves, *i.e.* from the intensity curves as a function of distance. Distances were converted into flight times by using the average velocities measured separately for the different nuclides without degrader foil. In this way the lifetime of the  $2_1^+$  state in  $^{60}\text{Fe}$  was determined to be 11.4(12) ps, which is in good agreement with the literature value of 11.6(22) ps [22]. Lifetimes for the  $2_1^+$  states in  $^{62}\text{Fe}$  and  $^{64}\text{Fe}$  were determined for the first time and found to be similar with 7.4(9) and 7.4(26) ps, respectively. The observed feeding times from the  $4^+$  states were found to be slightly different in  $^{62}\text{Fe}$  and  $^{64}\text{Fe}$ . The decay curves are consistent with the assumption of equal feeding times from the observed  $4^+ \rightarrow 2^+$  and other unobserved transitions. Systematic deviations of the lifetimes derived at individual distances would appear if the feeding times for observed and unobserved transitions were different. The measured lifetimes yield  $B(E2; 2_1^+ \rightarrow 0_1^+)$  values of 214(26) and  $470_{-110}^{+210} e^2\text{fm}^4$  for  $^{62}\text{Fe}$  and  $^{64}\text{Fe}$ , respectively.

The  $B(E2; 2_1^+ \rightarrow 0_1^+)$  values and excitation energies of the  $2_1^+$  states in this mass region are shown as a function of neutron number in the left part of Fig. 3. The large  $2_1^+$  energy and small  $B(E2)$  value for  $^{68}\text{Ni}$  could be interpreted as a sign for a sub-shell closure at  $N = 40$ . However, the chains of Zn and Fe isotopes above and below the proton shell closure, respectively, show a different behavior compared to the Ni isotopes. The drop in excitation energy of the  $2_1^+$  states, which is observed for all isotopic chains except Ni, illustrates that the nuclei become more collective and deformed with increasing neutron number. The  $B(E2)$  values show that collectivity develops more gradually in the Zn compared to the Fe isotopes, where the new data indicate a steep increase from  $^{62}\text{Fe}$  to  $^{64}\text{Fe}$ .

To understand the rapid onset of collectivity in  $^{64}\text{Fe}$  we have performed new shell model calculations beyond the scope of previous calculations in this mass region [30]. A large valence space was used comprising the  $fp$  shell for protons and the  $fpgd$  shell for neutrons outside a  $^{48}\text{Ca}$  core. The effective interaction was based on a realistic CD-Bonn potential adapted to the model space by many-body perturbation techniques [31] and modified in its monopole part. The interaction reproduces the global

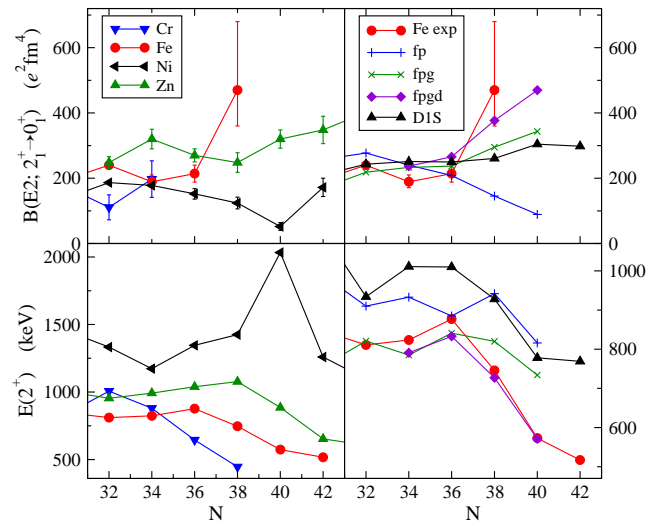


FIG. 3: Systematic of  $B(E2; 2_1^+ \rightarrow 0_1^+)$  and  $E(2_1^+)$  values for even-even nuclei around  $^{68}\text{Ni}$ . The data is taken from the compilation of Raman *et al.* [29] complemented by newer results for Cr [12, 21], Fe [11], Ni [23], and Zn [8] isotopes. The panels on the right compare the experimental results for the chain of Fe isotopes with theoretical calculations (see text).

evolution of single-particle energies along the nickel and  $N = 40$  isotopic and isotonic chains, respectively. Transition probabilities were obtained using a standard polarization effective charge of  $0.5e$ . The shell model diagonalizations accommodate for up to 14 particle-hole excitations across the  $Z = 28$  and  $N = 40$  gaps in the case of  $^{64}\text{Fe}$ . The largest dimensionality tackled in the study was  $7 \times 10^9$  for  $^{64}\text{Fe}$ . More details of the shell model calculations and the new effective interaction will be discussed in a forthcoming article [32].

To illustrate the importance of including the  $\nu g_{9/2}$  and  $d_{5/2}$  orbitals, calculations restricted to the neutron  $fp$  and  $fp$  valence spaces are also shown in Fig. 3. The comparison suggests that the  $fp$  valence space is sufficient to describe the  $2_1^+$  states in the Fe isotopes up to  $N = 36$ . The large  $B(E2; 2_1^+ \rightarrow 0_1^+)$  value measured for  $^{64}\text{Fe}$  clearly demonstrates the influence of neutron excitations across the gap at  $N = 40$ . In fact, the  $B(E2)$  value can only be explained if the  $d_{5/2}$  orbital is also included in the model space. The effect becomes even more evident in  $^{66}\text{Fe}$ : Only the calculations in the full  $fpgd$  model space reproduce the low excitation energies of the  $2_1^+$  state. It is well understood that the valence space should contain quasi-SU(3) partners, in this case the  $g_{9/2}$  and  $d_{5/2}$  orbitals, to allow the development of quadrupole collectivity [33].

For the ground state of  $^{64}\text{Fe}$  the  $fpgd$  shell model calculations find average occupancies for the  $\nu g_{9/2}$  and  $d_{5/2}$  orbitals of 1.76 and 0.21, respectively, and this state is characterized by an intruder configuration with a strong two-particle two-hole component. Such intruder configurations become completely dominant in  $^{66}\text{Fe}_{40}$  and also in  $^{62}\text{Cr}_{38}$ . In the latter case the occupancies of the  $g_{9/2}$

and  $d_{5/2}$  orbitals increase to 2.2 and 0.72, respectively, which drives the nucleus to an intrinsically deformed prolate shape (with  $\beta \approx 0.35$ ) and causes a more rotational yrast sequence consistent with experimental observations [13]. The transition from spherical  $^{68}\text{Ni}$  to more proton deficient  $N \approx 40$  isotones with deformed intruder configurations seems to have some similarity to the situation in the so-called *island of inversion* of Na and Mg isotopes with  $N \approx 20$  (see e.g. Ref. [1] for a review). In both cases the developing quadrupole collectivity can be related to the occupation of neutron intruder orbitals from the next oscillator shell, which are at the same time quasi-SU(3) partners:  $(f_{7/2}, p_{3/2})$  for  $^{32}\text{Mg}$  and  $(g_{9/2}, d_{5/2})$  in the present case. Active quadrupole partners are also available for the protons:  $(d_{5/2}, s_{1/2})$  for Mg and  $(f_{7/2}, p_{3/2})$  for Fe and Cr. The shell model calculations furthermore find a reduction in the harmonic oscillator gap at  $N = 40$  from  $^{68}\text{Ni}$  to  $^{60}\text{Ca}$ . The sudden increase of collectivity from  $^{62}\text{Fe}$  to  $^{64}\text{Fe}$  can thus be understood in a similar way as the increase of collectivity from  $^{30}\text{Mg}$  to  $^{32}\text{Mg}$ .

It is clear, on the other hand, that there is no shell closure at  $N = 40$  comparable to the one at  $N = 20$ . At this point the analogy between the island of inversion, which is situated at the end of a long chain of spherical  $N = 20$  isotones, and the  $N = 40$  region breaks down. With the exception of  $^{68}\text{Ni}$  with closed proton shell, all  $N = 40$  isotones develop collectivity and deformation (see left-hand part of Fig. 3). In a recent study within a microscopic collective model, the low-lying states in the  $N = 40$  isotones (except  $^{68}\text{Ni}$ ) were described as prolate deformed ground-state bands and quasi- $\gamma$  bands with good overall agreement between the calculations and experimental data [34]. We have extended these studies along the chain of Fe isotopes. The  $2_1^+$  energies and  $B(E2)$  values were obtained in Hartree-Fock-Bogolyubov based configuration mixing calculations using the the Gogny D1S force [35, 36] and the generator coordinate method with Gaussian overlap approximation, treating axial and triaxial quadrupole deformations [37]. The calculations use a triaxial harmonic oscillator basis including 11 major shells. The collective masses are calculated as described in Ref. [38]. Albeit the  $2_1^+$  energies are on average 30% too high, the systematic trend is reasonably well reproduced, considering that the model contains no free parameters (and no effective charges). The calculated  $B(E2)$  values show only a small increase at  $N = 40$ ,

which can also be attributed to the occupancy of the  $\nu g_{9/2}$  orbital. This occupancy is found to increase from approximately 0.6 in in the ground state of  $^{60}\text{Fe}$  to 2.5 in  $^{64}\text{Fe}$  [39]. The occupancy of the  $d_{5/2}$  orbital in the ground state of  $^{64}\text{Fe}$  is found to be 0.06, *i.e.* smaller than in the shell model. A more important difference, however, is the fact that the  $N = 40$  gap remains more or less constant in the Gogny mean-field calculation, performed at deformation zero, with  $\Delta E \approx 4$  MeV from  $Z = 20$  to  $Z = 40$  (see Fig. 1 in Ref. [34]), whereas in the shell model the gap is strongly reduced for  $Z < 28$ . Although it is not obvious that single-particle energies from shell model and spherical mean-field calculations can be directly compared, since the latter do not contain any correlations beyond the mean field, the different development of the  $N = 40$  shell gap could explain the more gradual increase of  $B(E2)$  values in the Gogny calculation. On the other hand, also proton excitations and the size of the  $Z = 28$  gap could contribute to the difference in collectivity. More theoretical work is needed to understand the origin of the differences between the shell model and mean-field predictions. While experimental data on  $^{60}\text{Ca}$  remain out of reach with present-day techniques, the measurement of  $B(E2)$  values in neutron-rich Cr isotopes will already shed more light on this question and allow making better predictions for a possible doubly-magic nature of  $^{60}\text{Ca}$ .

In summary, the lifetimes of the  $2_1^+$  states in  $^{62}\text{Fe}$  and  $^{64}\text{Fe}$  have been measured using the RDDS technique in combination with multi-nucleon transfer reactions in inverse kinematics. A steep increase of the  $B(E2; 2_1^+ \rightarrow 0_1^+)$  value is observed from  $^{62}\text{Fe}$  to  $^{64}\text{Fe}$ . The comparison with both shell model calculations and a microscopic collective model based on the Gogny force allows relating the increase in collectivity to the occupation of neutron intruder orbitals. The mechanism causing this onset of collectivity below  $^{68}\text{Ni}$  is found to be similar to the one responsible for the island of inversion around  $^{32}\text{Mg}$ . The two theoretical approaches predict a different structure of the more exotic nuclei with  $N \approx 40$ .

The authors would like to thank the technical staff at GANIL for excellent support and A. Navin for fruitful discussions. This work was partly supported by DFG (Germany) under Contract No. DE1516/-1.

- 
- [1] O. Sorlin, M.-G. Porquet, *Prog. Part. Nucl. Phys.* **61**, 602 (2008).  
 [2] T. Otsuka, T. Suzuki, R. Fujimoto, H. Grawe, Y. Akaishi, *Phys. Rev. Lett.* **95**, 232502 (2005).  
 [3] R. Broda *et al.*, *Phys. Rev. Lett.* **74**, 868 (1995).  
 [4] O. Sorlin *et al.*, *Phys. Rev. Lett.* **88**, 092501 (2002).  
 [5] C. Guénaut *et al.* *Phys. Rev. C* **75**, 044303 (2007).  
 [6] S. Rahaman *et al.*, *Eur. Phys. J. A* **34**, 5 (2007).  
 [7] K. Langanke, J. Terasaki, F. Nowacki, D.J. Dean,

- W. Nazarewicz, *Phys. Rev. C* **67**, 044314 (2003).  
 [8] J. Van de Walle *et al.*, *Phys. Rev. Lett.* **99**, 142501 (2007).  
 [9] E. Padilla-Rodal *et al.*, *Phys. Rev. Lett.* **94**, 122501 (2005).  
 [10] M. Hannawald *et al.*, *Phys. Rev. Lett.* **82**, 1391 (1999).  
 [11] P. Adrich *et al.*, *Phys. Rev. C* **77**, 054306 (2008).  
 [12] O. Sorlin *et al.*, *Eur. Phys. J. A* **16**, 55 (2003).  
 [13] N. Aoi *et al.*, *Phys. Rev. Lett.* **102**, 012502 (2009).

- [14] K. Kaneko, Y. Sun, M. Hasegawa, T. Mizusaki, Phys. Rev. C **78**, 064312 (2008).
- [15] N. Hoteling *et al.*, Phys. Rev. C **74**, 064313 (2006).
- [16] S. Lunardi *et al.*, Phys. Rev. C **76**, 034303 (2007).
- [17] M. Block *et al.*, Phys. Rev. Lett. **100**, 132501 (2008).
- [18] J.J. Valiente-Dobón *et al.*, Phys. Rev. C **78**, 024302 (2008).
- [19] H.L. Crawford *et al.*, Phys. Rev. C **79**, 054320 (2009).
- [20] S.J. Freeman *et al.*, Phys. Rev. C **69**, 064301 (2004).
- [21] A. Bürger *et al.*, Phys. Lett. **B622**, 29 (2005).
- [22] E.K. Warburton, J.W. Olness, A.M. Nathan, J.J. Kolata, J.B. McGrory, Phys. Rev. C **16**, 1027 (1977).
- [23] O. Perru *et al.*, Phys. Rev. Lett. **96**, 232501 (2006).
- [24] A. Dewald *et al.*, Z. Phys. A **334**, 163 (1989).
- [25] J.J. Valiente-Dobón *et al.*, Phys. Rev. Lett. **102**, 242502 (2009).
- [26] S. Pullanhiotan *et al.*, Nucl. Instr. Meth. A **593**, 343 (2008).
- [27] J. Simpson *et al.*, Acta Phys. Hung. N. S. **11**, 159 (2000).
- [28] T. Pissulla, A. Dewald *et al.*, Nucl. Instr. Meth. A, to be published.
- [29] S. Raman *et al.*, At. Data Nucl. Data Tables **78**, 1 (2001).
- [30] E. Caurier *et al.*, Eur. Phys. J. A **15**, 145 (2002).
- [31] M. Hjorth-Jensen, T.T.S. Kuo, E. Osnes, Phys. Rep. **261**, 125 (1995).
- [32] S.M. Lenzi *et al.* to be published
- [33] A.P. Zuker, J. Retamosa, A. Poves, E. Caurier, Phys. Rev. C **52**, R1741 (1995).
- [34] L. Gaodefroy *et al.*, Phys. Rev. C **80**, 064313 (2009).
- [35] J. Dechargé, D. Gogny, Phys. Rev. C **21**, 1568 (1980).
- [36] J.-F. Berger, M. Girod, D. Gogny, Comput. Phys. Commun. **63**, 365 (1991).
- [37] J.-P. Delaroche *et al.*, Phys. Rev. C **81**, 014303 (2010).
- [38] M. Zielińska *et al.*, Phys. Rev. C **80**, 014317 (2009).
- [39] J.M. Daugas *et al.*, to be published.